Bovine Serum Albumin Adsorption on SiO_2 and TiO_2 Nanoparticle Surfaces at Circumneutral and Acidic pH: A Tale of Two Nano-Bio Surface Interactions

Brittany E. Givens,[a#] Zhenzhu Xu,[b#] Jennifer Fiegel[a] and Vicki H. Grassian[c*]

[a]Department of Chemical & Biochemical Engineering, University of Iowa, Iowa City, IA 52242

[b]Department of Chemistry, University of Iowa, Iowa City, IA 52242

[c]Department of Chemistry & Biochemistry, Nanoengineering and Scripps Institution of Oceanography, University of California San Diego, La Jolla CA 92037

Abstract

The interaction of a model protein, bovine serum albumin (BSA) with two different metal oxide nanoparticles, TiO_2 (~22 nm) and SiO_2 (~14 nm), was studied at both physiological and acidic pH. The pH- and nanoparticle-dependent differences in protein structure and protein adsorption were determined using attenuated total reflectance Fourier transform infrared spectroscopy (ATR-FTIR) and thermogravimetric analysis (TGA). The results indicated that the surface coverage of BSA decreases with decreasing pH on both TiO_2 and SiO_2 surfaces, and BSA coverage is higher by a factor of ca. 3 to 10 times more on TiO_2 compared to SiO_2. The secondary structure of BSA changes upon adsorption to either nanoparticle surface at both pH 7.4 and 2. At acidic pH, BSA appears to completely unfold on TiO_2 nanoparticles whereas it assumes an extended conformation on SiO_2. These differences highlight for the first time the extent to which the protein corona structure is significantly impacted by protein-nanoparticle interactions which depend on the interplay between pH and specific nanoparticle surface chemistry.

Co-first authors

* Author to whom correspondence should be addressed

Metal oxide nanoparticles have been used in several industries and consumer products. Two metal oxides in particular, TiO_2 and SiO_2, have a broad range of applications and are among the most prevalent metal oxide nanoparticles used.[1,2] For example, both TiO_2 and SiO_2 nanoparticles are critical materials in pigments and both are used as food additives.[3-8] Although these metal oxide nanoparticles bring significant benefits, their widespread use also makes them of interest as a potential risk to human health and the environment.[9,10] There is evidence showing that nanoparticles, upon uptake by biological targets, could generate reactive oxygen species (ROS) and induce oxidative stress which could be harmful to the cell membrane and cause DNA damage.[9-12] Moreover, as discussed in detail below, when proteins adsorb to nanoparticle surfaces there is a potential for protein denaturation which may cause loss of protein function.[13]

In biological systems, a layer of proteins forms at the nanoparticle surface. This is called the protein corona; the protein corona includes proteins, lipids, and ions that immediately adsorb to the nanoparticle surface,[14-18] and it is a dynamic entity that can change over time.[15,19] Studies have investigated the kinetic and thermodynamic properties of corona formation, as well as the composition of the corona in simple and complex media.[15,20-23] Determining which proteins adsorb to the surface, and how their structure changes, is difficult in complex media.

The most common model protein for simplified systems is bovine serum albumin (BSA). Although there have been several studies on the adsorption of BSA on various inorganic and polymeric nanoparticle surfaces, including metal oxide nanoparticles in biological media,[24-26] few have investigated the pH-effects of this adsorption process.[27-30] Since oxide nanoparticles are common in both food additives as well as topical products, there needs to be an understanding of the protein corona under different conditions as pH varies widely across the gastrointestinal tract

from pH 1-3 in the stomach, to 5-6 in the large intestines, and 7-8 in the small intestine.[31] Therefore, it is very important to evaluate the environmental health and safety of SiO_2 and TiO_2 nanomaterials as a f(pH).

BSA has a molecular weight of approximately 66 kDa,[32] and is widely used as a model protein because it has similar properties, molecular weight, and an amino acid sequence to its human variant, human serum albumin, it is easily available, and albumin is ubiquitous in the body, found in all bodily fluids.[33] It has been demonstrated that BSA exists in multiple forms depending on the pH of its environment, as shown in Figure 1. The common forms of BSA are the normal form (N form, pH 9.0-4.5), the fast form (F form, pH 4.0-3.5), and the extended form (E form, pH below 3.5). Between pH 4.5-4.0, BSA exists in an N-F transition form and abruptly transforms to the F form when the pH drops below 4.0. The 3-D sizes of N, F, and E forms of BSA are: 8.0 × 8.0 × 3.0 Å, 4.0 × 4.0 × 12.9 Å, and 2.1 × 2.1 × 25.0 Å, respectively.[34,35] The structure of BSA gradually lengthens from N form to E from. Thus, conformational changes occur in both the secondary and tertiary protein structure as a function of solution pH. BSA can also undergo changes in conformation upon surface adsorption.[13,36,37] There is evidence that BSA adsorption is optimal at its experimental isoelectric point, 4.7 at room temperature.[28,38] However, a systemic study of BSA behavior at different pH on nanoparticle surfaces is still lacking, especially at low pH.

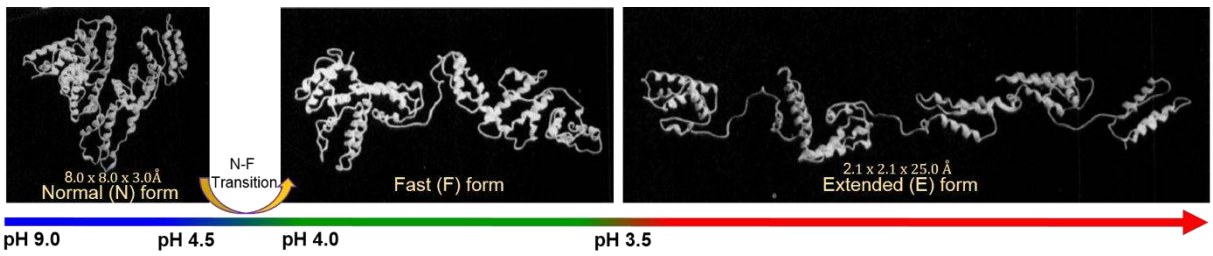

Figure 1. Diagram of BSA form and dimension changes as a function of pH (Modified from Carter, D. C.; Ho, J. X., 1994. With permission from Elsevier.).[35]

To investigate changes in protein structure upon adsorption on to nanoparticle surfaces at circumneutral and acidic pH, we have used attenuated total reflectance-Fourier transformation infrared (ATR-FTIR) spectroscopy. This tool provides a real-time, *in situ* analysis of the nanoparticle-protein interface.[18,39,40] We are able to probe this nanoparticle-protein interface due to the evanescent wave that extends upon each internal reflection and the transparency of the metal oxide nanoparticles in the spectral region of interest.[18,41] Infrared absorption bands in the region from 1600 – 1700 cm^{-1} are most often used for secondary structure determination because it has high absorbance intensity and is comprised from amino acid functional groups which determine the hydrogen bonding interactions of the secondary structure[42] Complementing the ATR-FTIR spectroscopic data, we use thermogravimetric analysis (TGA) to determine the surface coverage of BSA on the nanoparticle surface.[43,44] In this work, we quantitatively compare the adsorption and conformation of BSA on two metal oxide nanoparticle surface thin films composed of SiO_2 and TiO_2. These data allow us to make predictions as to the effects of nanoparticles on protein structure and function circulating in the blood at circumneutral pH, and in the stomach as released from food additives at acidic pH.

Results and Discussion

Nanoparticle Characterization. TiO_2 primary nanoparticle size was determined to be 22 ± 1 nm whereas SiO_2 nanoparticle size was determined to be 14 ± 2 nm from transmission electron microscopy (TEM). The surface area of SiO_2 was 330 ± 24 m^2/g whereas that for TiO_2 was 50 ± 8 m^2/g as determined from BET analysis; both agree well with company specifications for these particles. Additionally, phase state was determined for these nanoparticles. SiO_2 nanoparticles were amorphous, and the X-ray diffraction (XRD) pattern for TiO_2 particles shows that TiO_2 was 86% anatase and 14% rutile. Furthermore, isoelectric point (IEP) for SiO_2 and TiO_2

nanoparticles were obtained by running zeta potential measurements and plotting zeta potential as a function of pH. The experimentally determined isoelectric point for SiO_2 and TiO_2 nanoparticles are 3.1 and 6.5 respectively which are consistent with literature reported values that are ~pH 3.0 and ~pH 7.0 respectively.[45,46] These data are summarized in Table 1 and additional data (TEM images, XRD and zeta potential measurements) are shown in Supporting Information (Fig. S1 and Fig. S2).

Table 1. A summary of nanoparticle characterization data from TEM, BET, XRD measurements and IEP assessment.

Nanoparticle	TEM determined size (nm)	BET surface area (m^2/g)	Crystallinity	IEP
SiO_2	14 ± 2	330 ± 24	Amorphous	3.1
TiO_2	22 ± 1	50 ± 8	86% anatase 14% rutile	6.5

ATR-FTIR spectroscopy of BSA in solution at pH 7.4 and pH 2.0 The characteristic IR absorption bands for proteins are commonly referred to as the amide I, II, and III regions. The amide I region exhibits peaks from the C=O stretch and extends from 1600-1700 cm^{-1}. The amide II region arises from the combined motions of the C-N stretch and the N-H bend and ranges from 1500-1600 cm^{-1}. The amide III region commonly has multiple smaller peaks, but is primarily composed of CH_2 scissoring motion. The amide III region extends from 1200-1350 cm^{-1}.The ATR-FTIR spectra for 10 mg/mL BSA in solution at pH 7.4 and pH 2.0 in the amide regions is presented in Figure 2.[18,47-50] At pH 2 there is an additional peak at 1712 cm^{-1} which corresponds to a carbonyl stretch associated with the protonation of COO^- groups in amino acids to form COOH.[18,51] At pH 7.4 there is an additional peak at 1399 cm^{-1} which is due to the deprotonated form and is associated with the C-O carboxylate stretch.[49] The spectra shown in Figure 2 agree with previous studies on BSA in solution as a function of pH.

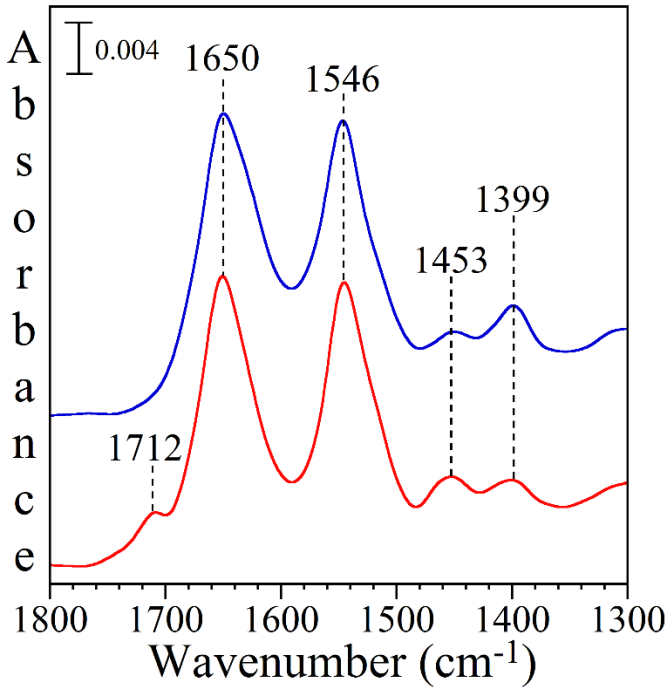

Figure 2. Absorbance spectra of 10 mg/mL BSA solution at pH 7.4 (top) and pH 2.0 (bottom) in the amide regions. Peaks shown are for protonated carboxyl group at pH 2.0 (1712 cm^{-1}), the amide I peak (1650 cm^{-1}), amide II peak (1546 cm^{-1}) and the amide III region (peaks 1453 and 1399 cm^{-1}).

ATR-FTIR spectroscopy of BSA adsorbed on SiO_2 and TiO_2 at pH 7.4 and pH 2.0. As BSA adsorbed to the nanoparticle surfaces over time, the absorption band intensities increased in the amide regions. There were also small shifts in frequency due to changes in the interaction with the surface and other co-adsorbed BSA molecules. In particular, shifts to lower wavenumbers are often due to increased hydrogen bonding,[52] and shifts to higher wavenumbers are indicative of increased beta structures.[53] Figure 3 displays the ATR spectra for BSA adsorption to nanoparticle surfaces over time at pH 7.4 (3a) and pH 2.0 (3b). Smaller peak shifts from the initial time to the final time were observed for SiO_2 than for TiO_2. Additionally, adsorption of BSA appears to be greater on the TiO_2 surface compared with the SiO_2 surface, as noted by the difference in absorbance intensity between substrates.

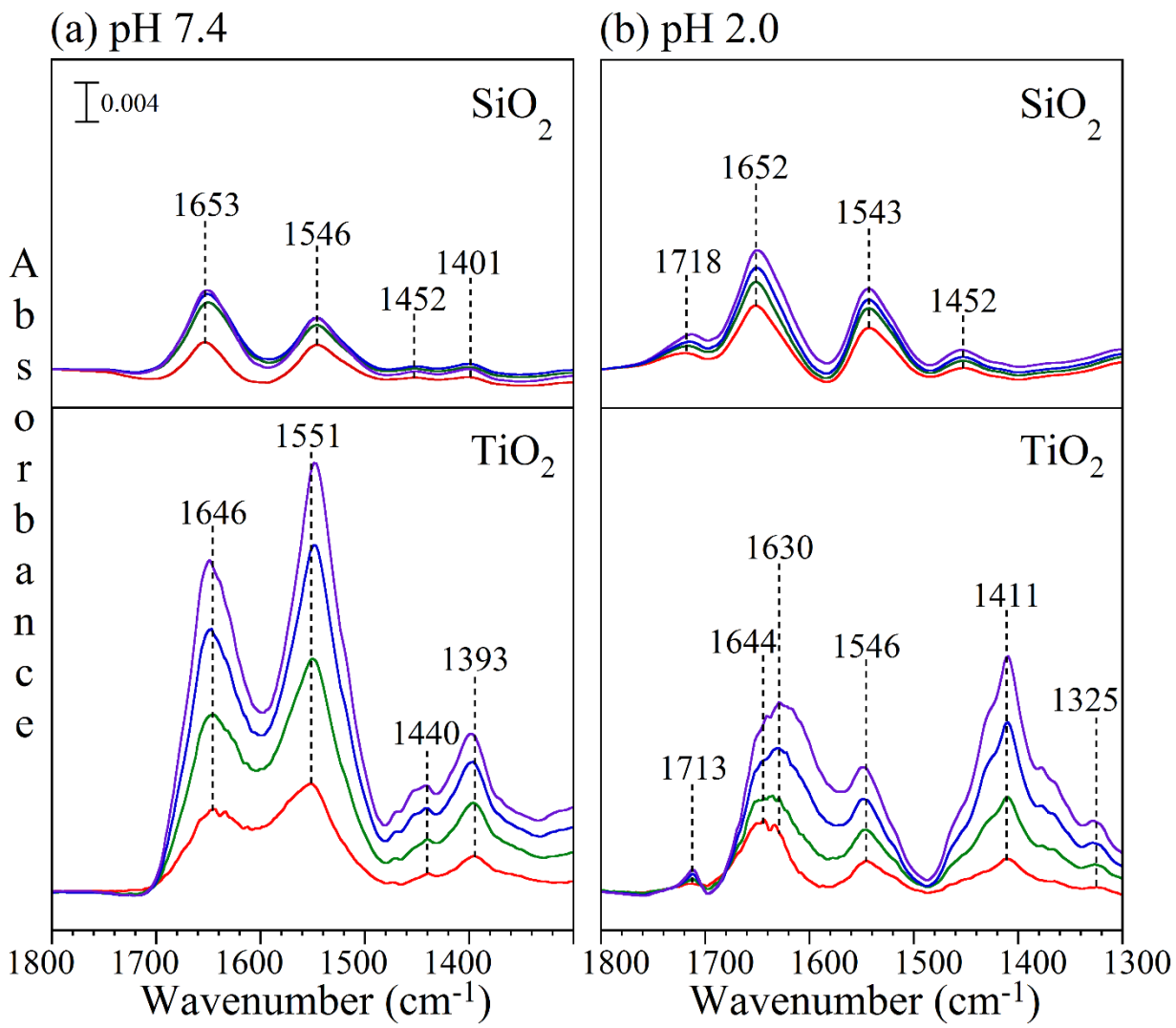

Figure 3. Absorbance spectra of 1 mg/mL BSA as a function of time for (a) pH 7.4 on SiO_2 nanoparticles (top) and TiO_2 nanoparticles (bottom), (b) pH 2.0 on SiO_2 nanoparticles (top) and TiO_2 nanoparticles (bottom). Spectra are shown for four different time points: 10, 30, 60, and 90 minutes (bottom to top).

At both pH the spectra for BSA adsorbed onto SiO_2 exhibited relatively consistent peak frequencies, whereas on TiO_2 at pH 2.0 the bands exhibited enhanced relative band intensity, band broadening, and shifts in frequency for each of the bands in the spectrum. These changes indicate that the protein was unfolding and/or denaturing on the surface.[13,54] A new peak at 1411 cm^{-1} appeared under this condition which can be attributed to the symmetric stretching mode of

COO^- in BSA attached to the highly hydroxylated TiO_2 surface at acidic pH.[18,55,56] The separation of the peak at 1646 cm^{-1} into peaks at 1644 and 1630 cm^{-1} arises from the asymmetric stretching mode of NH_3^+ in highly charged amino acids of BSA.[18,56]

Absorbance intensity between the amide I and amide II peaks can give qualitative information on the protein secondary structure.[36] The ratio of relative intensities of the amide I and amide II peaks, that is, the amide I/II ratio changes upon adsorption on both particle surfaces. Combined with the knowledge of amide I peak shifts, the amide I/II ratio implies BSA conformation changes differed because of the different surfaces and pH. More specifically, it can be derived that the conformational change comes in the form of beta and turn structures as reported in previous studies.[53]

Secondary protein structural analyses of BSA in solution and adsorbed on SiO_2 and TiO_2. To further determine changes in protein structure upon adsorption, spectra for BSA in the solution phase, adsorbed on TiO_2 nanoparticles, and adsorbed on SiO_2 nanoparticles at pH 7.4 and pH 2.0 were curve fit. To learn more about how the secondary structure changes upon adsorption at two different pH. The amide I band was curve fit using five components for the secondary structure of BSA according to five literature-reported component bands, as summarized in Table 2.[13,36,57] The normalized curve fit amide I bands are presented in Figure 4, where the black line represents the original spectrum and the light blue or red dotted lines represent the overall fit at pH 7.4 and pH 2.0, respectively. The percent content for each of the secondary structure elements is reported in Table 3. Literature values for secondary structure elements of BSA vary over a range of approximately 10%, however most agree the alpha helix content is 60-65% of the total secondary structure.[43,57-62] For our studies, changes greater than 10% upon adsorption were considered significant given this variability.

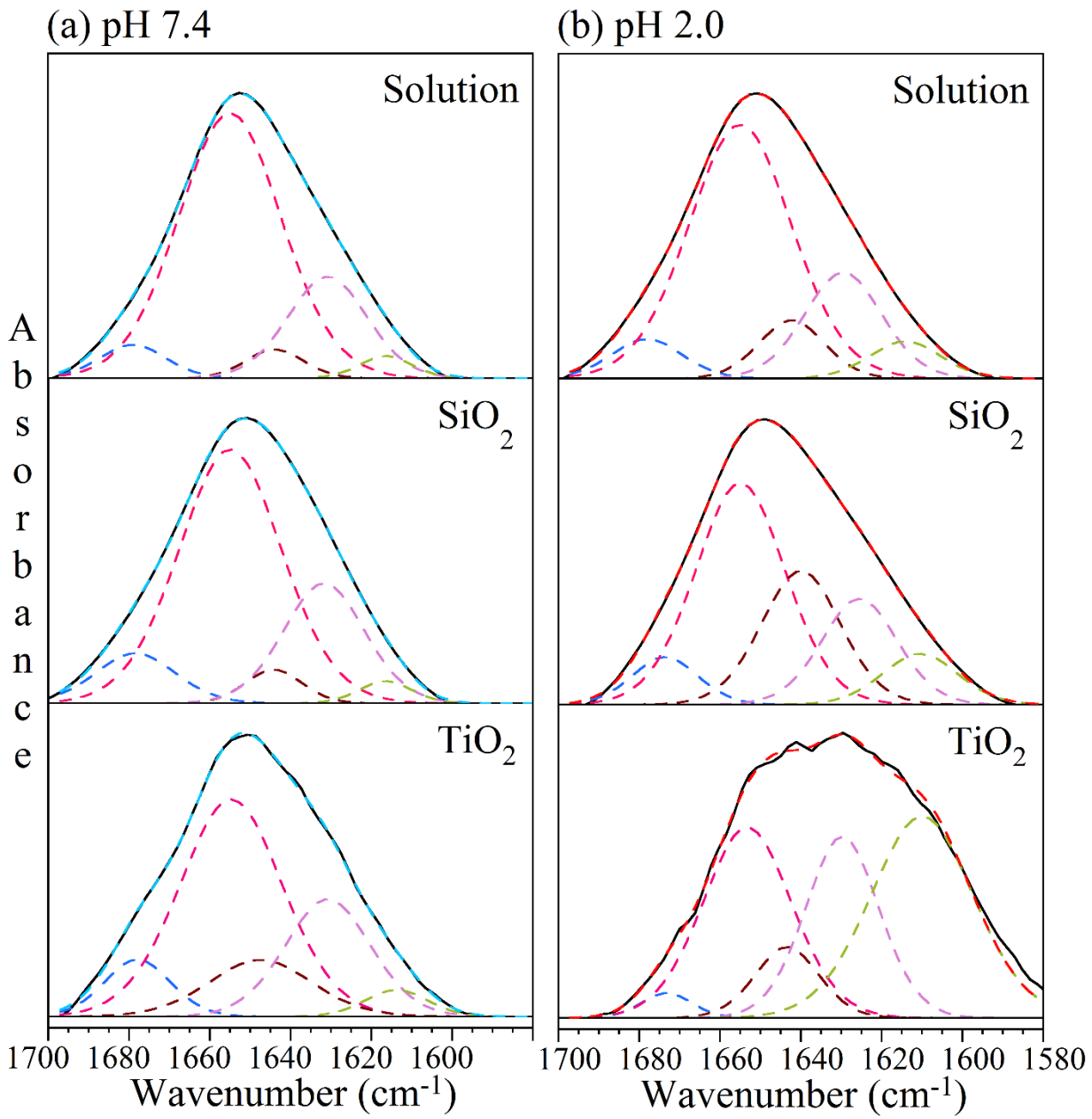

Figure 4. Background subtracted and normalized BSA amide I band for secondary structural analysis curve fitting for structural analysis: (a) 10 mg/mL BSA solution (top), adsorbed BSA on SiO_2 nanoparticles (middle) and adsorbed BSA on TiO_2 nanoparticles (bottom) at pH 7.4; (b) 10 mg/mL BSA solution (top), adsorbed BSA on SiO_2 nanoparticles (middle) and adsorbed BSA on TiO_2 nanoparticles (bottom) at pH 2.0. The black lines represent the original experimental spectrum and the light blue or red dotted lines represent the overall fit at pH 7.4 and pH 2.0, respectively. Component bands are given for β-sheets/turns (dark blue), α-helices (dark pink), random chains (dark red), extended chains/β-sheets (light pink), and side chain moieties (lime).

Table 3. Vibrational frequencies of the absorption bands associated with secondary structural elements of BSA in the amide I region used for curve fitting.

Secondary structure	Vibrational frequency (cm^{-1})
β-sheets/turns	1685-1663
α-helices	1655-1650
Random chains	1648-1644
Extended chains/β-sheets	1639-1621
Side chain moieties	1616-1600

Table 4. The secondary structure content (%) in BSA determined via curve fitting for BSA in solution and after adsorption on to the nanoparticle surfaces; SiO_2 and TiO_2.

pH	Secondary structure	Solution phase BSA	Adsorbed BSA on SiO_2 (Δ from solution)[a]	Adsorbed BSA on TiO_2 (Δ from solution)[a]
7.4	β-sheets/turns	5	9 (+4)	9 (+4)
	α-helices	68	59 (-9)	51 (-17)
	Random chains	4	15 (+11)	13 (+9)
	Extended chains/β-sheets	20	12 (-8)	23 (+3)
	Side chain moieties	3	5 (+2)	4 (+1)
2.0	β-sheets/turns	6	5 (-1)	2 (-4)
	α-helices	60	48 (-12)	30 (-30)
	Random chains	9	15 (+6)	8 (-1)
	Extended chains/β-sheets	19	25 (+16)	24 (+15)
	Side chain moieties	6	7 (+1)	36 (+30)

[a] – difference between adsorbed and solution phase structure content

In solution, BSA had a decreased α-helix content at pH 2.0 compared with the physiological pH 7.4, which is consistent with the literature.[63,64] The same was true for BSA adsorbed on either nanoparticle surface. However, there was more than double the amount of α-helix content loss in BSA upon adsorption to the TiO_2 surface compared with adsorption to the SiO_2 surface at pH 2.0. In contrast, at pH 7.4, α-helix content decreased upon adsorption and the

random chain content increased on both SiO_2 and TiO_2 nanoparticles. Loss of helical structure is greater for TiO_2 than for SiO_2, and SiO_2 undergoes a loss of extended chains/β -sheets.

In general, the loss of α-helical structure is expected to be balanced by an increase in β-structures.[36] However, for BSA on TiO_2 at pH 2.0 which exhibited the greatest loss in α-helix structure compared to the solution phase, the major increase was in the side chain moieties rather than the β-structures. This suggests that more of the amino acid side chains of BSA were exposed and thus BSA denatured under these conditions. In contrast, with BSA on SiO_2 at pH 2.0, the majority of structural increase occurred in β-structures and relatively no change in side chain moieties were observed. Therefore, on SiO_2 there were changes in protein folding, but the protein remains intact and close to the native form.

These data on the change of secondary structure contents indicated that the highly helical structure of BSA unfolded in solution and further upon adsorption at lower pH. This manifested as a decreased α-helical content in the protein secondary structure. BSA had the highest alpha-helical content in solution at physiological pH, in its normal form.[13 65,66] In general, BSA lost more alpha helical structure upon adsorption on TiO_2 compared to on SiO_2 at the same pH. This was consistent with the relative shifts in the frequency of the absorption bands, where on SiO_2 there were smaller shifts compared with TiO_2. However, compared to solution phase BSA, the adsorbed BSA spectra on both surfaces experienced IR frequency shifts and large changes in the relative intensities which can be attributed to strong hydrogen bonding with the hydroxyl (–OH) groups on the surface.[52,55] On the TiO_2 surface at acidic pH, BSA lost the majority of the helical content which is consistent with protein unfolding on the surface and was not seen on SiO_2. Previous research showed loss of alpha helix structure is complemented by the gain of beta structures at neutral pH because of the relative stability of beta structures compared with alpha

helical structures.[36] In our studies, this was seen predominately in the chain structure of our protein upon adsorption to either nanoparticle surface. A recent study of BSA adsorption onto various types of SiO_2 nanoparticles indicated that BSA adsorbed onto non-porous particles results in a significant loss in alpha helix structure (10% remaining) and an increase in all other structures.[43] This study used complex medium (Roswell Park Memorial Institute, RPMI) rather than pure water, introducing a variety of other inorganic and biological components with the ability to adsorb to the SiO_2 surface.[43] Furthermore, the type of silica studied differed which has been shown to have an impact on its surface chemistry and toxicity.[67]

The greater denaturation effects on BSA adsorbed to the TiO_2 surface may be a result of stronger electrostatic interactions between BSA and the hydroxyl groups on TiO_2 surface. Both nanoparticles have –OH groups on their surfaces once hydrated which can interact with the adsorbed protein. As the number of surface hydroxyl groups increases, the affinity for the protein to the surface gets stronger.[55,68,69] It has been reported in the literature that TiO_2 nanoparticle surfaces have greater –OH density than SiO_2 surfaces,[68] therefore, BSA would have a higher binding strength on TiO_2 due to the increased number of interactions with OH groups. Electrostatic interactions with the surface have also been reported to play a critical role in protein adsorption, particularly between the $–COO^-$ and $–NH_3^+$ groups from the amino acid chain with the surface and surface charge depending on pH.[70]

Furthermore, there have been discussions on differences between a soft and a hard protein corona. The soft corona contains proteins that adsorb quickly, but reversibly, to the nanoparticle surface while the hard corona is characterized by proteins which adsorb slowly and irreversibly.[17,71] Proteins in the hard corona tend to undergo greater alterations in structure as compared with proteins in the soft corona.[71,72] Since the protein corona is substrate-dependent,[15]

and the ATR absorbance intensity indicates a much lower amount of BSA on the SiO_2 surface than the TiO_2 surface, it is likely that BSA is a soft corona component on SiO_2 and does not undergo structural changes. However, the same protein may be part of the hard corona on TiO_2 supported by the significant structural changes due to the conformational entropy of the protein on the TiO_2 surface.[72]

TGA of protein surface coverage on SiO_2 and TiO_2 nanoparticles. Additional quantitative information can be obtained from surface coverage measurements using thermal desorption of the protein from the nanoparticle surfaces; these data are summarized in Table 5. After 24 hours at 4°C, the surface was assumed to be saturated with BSA, but this does not account for the possibility of multi-layer adsorption. BSA adsorption was greater for pH 7.4 as compared to pH 2 on both nanoparticle surfaces. At physiological pH, BSA displayed an order of magnitude increase in adsorption to TiO_2 over SiO_2. Literature values for BSA adsorption onto SiO_2 at neutral pH exceed the observed values in this study ($4.5x10^{11}$, 4.8 ± 0.3 $x10^{11}$, and $1.09x10^{12}$ molecules cm^{-2}).[24,25,41] The literature reported value for BSA on TiO_2 falls slightly above the more common value for BSA on SiO_2, $5.7x10^{11}$ molecules cm^{-2}.[54] The nanoparticle types used in other studies vary slightly from those used in this study, and therefore variability in the quantification is expected. Overall, we conclude the values obtained from these experiments were consistent with the literature and with the ATR-FTIR absorbance intensity obtained with these systems.

The observed differences in adsorption as a function of nanoparticle surfaces and pH can be attributed to the availability of binding sites for hydrogen binding between protein and nanoparticle surface.[73,74] Anatase and rutile have different Ti atom densities which results in different surface density of –OH binding sites,[75,76] therefore the anatase/rutile ratio affects the

degree of BSA binding in these TiO_2 nanoparticles as compared with others in the literature. In general, anatase has a greater amount of protein adsorption relative to rutile.[77] In general, mixed phase samples have shown small rutile crystallites amongst the more abundant anatase phase.[78,79] SiO_2 nanoparticles have a lower surface hydroxyl density of about one half as compared with TiO_2 nanoparticles.[68] This is presented in a significantly lower adsorption of BSA to the SiO_2 surface than the TiO_2 surface as measured with TGA. The solution pH also plays an important role in the relative adsorption of BSA to the nanoparticle surfaces. The terminal hydroxyl groups on the TiO_2 surface are diminished at low pH and replaced with Ti-OH_2^+ or Ti-OH^+-Ti groups.[73]

Table 5. Surface coverage determination using thermogravimetric analysis (molecules/cm^2) of BSA adsorbed on SiO_2 and TiO_2.

	Surface coverage (molecules/cm^2)	
	pH 7.4	**pH 2.0**
BSA on SiO_2	$1.9 \pm 0.3 \times 10^{11}$	$1.5 \pm 0.2 \times 10^{11}$
BSA on TiO_2	$1.7 \pm 0.3 \times 10^{12}$	$4.6 \pm 0.7 \times 10^{11}$

Just as the surface point of zero charge has been shown to enhance adsorption,[27,53] protein adsorption has also been shown to be optimal at the isoelectric point of the protein.[24,73] This suggests that surface coverage is pH-dependent, and this dependence arises from a combination of the surface and the protein point of zero charge. Alternatively, the different dimensions of E-form BSA and N-form BSA results in different occupation of surface sites per molecule upon adsorption and, thus, gives a lower surface coverage at acidic pH.[12] This second effect is a potential new mechanism for understanding changes in protein coverages at different pH.

Conclusions

SiO_2 and TiO_2 nanoparticles are important metal oxides nanomaterials that are widely used in industry and consumer products. Even though these two types of nanomaterials are applied in common products, this study shows that these two nanomaterials could interact distinctively with the same protein as a function of pH. These results bring up some important factors in protein interaction with similar metal oxide nanoparticles and give insights into the environmental health and safety consideration when using nanomaterials in industry and consumer products. Several important conclusions come from this study of BSA adsorption on two different nanoparticle surfaces. These include:

1. Protein conformation changes as a function of pH both in solution and when adsorbed onto nanoparticle surfaces.
2. Protein conformation differs on the two oxide surfaces compared to that of solution at pH 7.4 and 2.0.
3. Protein interaction is strongest with the TiO_2 nanoparticle surface as indicated by the increased surface coverage and the larger change in protein conformation from solution when compared to SiO_2.

These effects have been summarized in Figure 5 and when taken together demonstrate that metal oxide nanoparticle surfaces impact protein structure. These structural changes are a function of function of nanoparticle surface chemistry and solution pH.

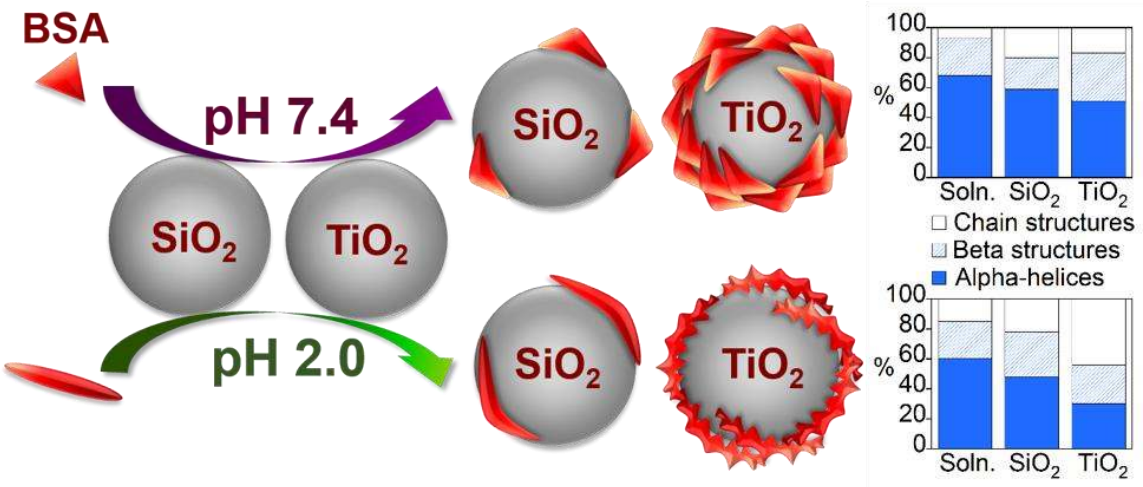

Figure 5. A summary of the experimental design and the effects of BSA adsorption onto metal oxide nanoparticle surfaces. BSA was added to solution at pH 7.4 or pH 2.0 and flowed over a nanoparticle surface, SiO_2 or TiO_2. Subsequently, BSA adsorbed to the nanoparticle surface in different quantities as measured by TGA and changed conformation to different extents as determined by curve fitting the ATR-FTIR spectra.

Methods

Nanoparticle characterization. Cab-O-Sil, a nonporous, amorphous hydrophilic fumed silica, was obtained from the Cabot Corporation and crystalline TiO_2 nanoparticles were purchased from Sigma-Aldrich. Transmission electron microscopy (TEM, JEOL JEM-1230) was used to determine the size and size distribution of individual nanoparticles with ImageJ software. A 100 μg/mL solution of nanoparticles in isopropanol (SiO_2) or ethanol (TiO_2) was prepared and sonicated for several minutes. Samples were deposited dropwise onto TEM copper grids and allowed to dry before imaging. Nanoparticle surface area was determined using 7-point Brunauer-Emmett-Teller (BET) analysis (Quantachrome BET Nova 4200e). Nanoparticles were allowed to degas at 300°C overnight before analysis. For crystalline phases in TiO_2, powder X-ray diffraction (XRD, Bruker D8 Advance) was used.

Zeta potential measurements. Laser Doppler velocimetry (Beckman-Coulter Nano C and Zetasizer Nano ZS90) was used to determine the zeta potential as a function of pH for SiO_2 and

TiO_2 nanoparticles and herein determine the isoelectric point for each material. Samples were prepared by mixing 5 mg of SiO_2 or TiO_2 with 5 mL of Optima water (Fisher Chemical) and adjusted to the desired pH with 1 M hydrochloric acid (HCl) and 0.8 M sodium hydroxide (NaOH) solutions. Measurements in the presence and absence of 1 mg/mL of BSA (98% purity, Sigma-Aldrich) were obtained across a wide range of pHs, including those of interest at pH 2.0 and 7.4. Samples were run in triplicate and conditions were duplicated to ensure reliability. The zeta potential versus pH curves that determine the isoelectric point for SiO_2 and TiO_2 are provided in the supporting information (Figure S2).

Attenuated Total Reflectance Fourier Transform Infrared (ATR-FTIR) spectroscopy. ATR-FTIR spectra of 10 mg/mL and 1 mg/mL BSA solutions at pH 2.0 and pH 7.4 exposed to the uncoated reflectance element were taken. For surface adsorption studies, thin films of nanoparticles on the ATR crystal were prepared by preparing solutions containing 2.5 mg TiO_2 or 8.0 mg SiO_2 in 1 mL Optima water (Fisher Chemical), sonicating the solutions for five minutes to form a uniform suspension, depositing the solutions on the AMTIR crystal element, and allowing the element to dry overnight. A horizontal flow cell (PIKE Technologies) was used to slowly flow (~1 mL/min) Optima water at the pH of interest above the nanoparticle thin film to remove loosely bound particles and to collect a background spectrum. Then a solution containing BSA (Sigma-Aldrich; 1 mg/mL; pH 2.0, pH 7.4) was introduced and a slow flow over the nanoparticle coated crystal was established while collecting spectra every ten minutes for one and a half hours.

A spectrum of water on the nanoparticles at the pH of interest was subtracted from the time-dependent spectra in the presence of BSA. The resulting spectra were fit to a Gaussian-Lorentzian shape with five component bands for the amide I region which arise from the

secondary structure of the protein's backbone. First, the solution phase spectrum of native BSA at 10 mg/mL was fit at pH 7.4 according to second derivative minima and literature constraints for the secondary structure elements, and likewise at pH 2.0.[12, 37] Second, the fitted components from the solution phase were used as initial guesses to fit the respective adsorbed phase on each nanoparticle surface. All spectra were modified to follow a linear baseline and maximum peak height equal to 1.0 to allow for direct comparisons at all conditions.

Thermogravimetric Analysis (TGA) of BSA Adsorption. Samples were run in triplicate with 4 mg SiO_2 or 2.5 mg TiO_2 and 1 mL of a 1 mg/mL BSA solution. The samples were sonicated for 20 minutes to form a uniform suspension. Then, samples were incubated at 4°C for 24 hours to reach saturation, prevent denaturation effects from temperature, and limit bacterial growth that may occur at higher temperatures. After incubation, each sample was washed three times with pure water by centrifuging at 10,000 rpm for 20 minutes and removing the supernatant. Washed samples were allowed to dry completely in a fume hood (2-3 days). The dried samples were crushed into a fine powder and loaded into a TGA instrument (Pyris 1 TGA, Perkin-Elmer). Samples were heated from 25°C – 700°C at a rate of 5°C per minute. The initial mass was taken at 100°C to remove and adsorbed water and the mass lost due to protein desorption were taken from 100°C - 600°C.

Acknowledgements

This work was supported by the National Science Foundation (Grant CBET1640936). Any opinions, findings and conclusions or recommendations expressed in this material are those of the authors and do not necessarily reflect those of the National Science Foundation. We would like to thank Professor Allan Guymon laboratory at the University of Iowa in the Department of Chemical and Biochemical Engineering for use of the TGA instrument and Professor Michael J.

Sailor laboratory at the University of California, San Diego in the Department of Chemistry and Biochemistry for the zeta potential measurements. We also thank Sanjaya Jayalath for characterization data for some of the nanomaterials used in this study. Additional support for Brittany E. Givens was provided by the Alfred P. Sloan Foundation through the University of Iowa Center for Exemplary Mentoring. We also acknowledge helpful discussions with Professor Sarah C. Larsen, Dr. Imali A. Mudunkotuwa and Dr. Sean E. Lehman during the course of this work.

References

(1) Lee, J.; Mahendra, S.; Alvarez, P. J. *ACS Nano* **2010**, *4*, 3580.

(2) Zhang, H.; Ji, Z.; Xia, T.; Meng, H.; Low-Kam, C.; Liu, R.; Pokhrel, S.; Lin, S.; Wang, X.; Liao, Y.-P. *ACS Nano* **2012**, *6*, 4349.

(3) Long, T. C.; Saleh, N.; Tilton, R. D.; Lowry, G. V.; Veronesi, B. *Environmental Science & Technology* **2006**, *40*, 4346.

(4) Macwan, D.; Dave, P. N.; Chaturvedi, S. *Journal of Materials Science* **2011**, *46*, 3669.

(5) Shi, H.; Magaye, R.; Castranova, V.; Zhao, J. *Particle and Fibre Toxicology* **2013**, *10*, 15.

(6) Lin, W.; Huang, Y. W.; Zhou, X. D.; Ma, Y. *Toxicology and Applied Pharmacology* **2006**, *217*, 252.

(7) Patwardhan, S. V.; Emami, F. S.; Berry, R. J.; Jones, S. E.; Naik, R. R.; Deschaume, O.; Heinz, H.; Perry, C. C. *Journal of the American Chemical Society* **2012**, *134*, 6244.

(8) Lomer, M. C. E.; Thompson, R. P. H.; Powell, J. J. *The Proceedings of the Nutrition Society* **2002**, *61*, 123.

(9) Oberdörster, G.; Oberdörster, E.; Oberdörster, J. *Environmental Health Perspectives* **2005**, *7*, 823.

(10) Warheit, D. B.; Sayes, C. M.; Reed, K. L.; Swain, K. A. *Pharmacolology and Therapeutics* **2008**, *120*, 35.

(11) Jani, P. U.; McCarthy, D. E.; Florence, A. T. *International Journal of Pharmaceutics* **1994**, *105*, 157.

(12) Stone, V.; Johnston, H.; Clift, M. J. *IEEE Transactions on NanoBioscience* **2007**, *6*, 331.

(13) Roach, P.; Farrar, D.; Perry, C. C. *Journal of the American Chemical Society* **2005**, *127*, 8168.

(14) Lesniak, A.; Fenaroli, F.; Monopoli, M. P.; Aberg, C.; Dawson, K. A.; Salvati, A. *ACS Nano* **2012**, *6*, 5845.

(15) Lundqvist, M.; Stigler, J.; Cedervall, T.; Berggard, T.; Flanagan, M. B.; Lynch, I.; Elia, G.; Dawson, K. *ACS Nano* **2011**, *5*, 7503.

(16) Lundqvist, M.; Stigler, J.; Elia, G.; Lynch, I.; Cedervall, T.; Dawson, K. A. *Proceedings of the National Academy of Sciences of the United States of America* **2008**, *105*, 14265.

(17) Lynch, I.; Dawson, K. A. *Nano Today* **2008**, *3*, 40.

(18) Mudunkotuwa, I. A.; Al Minshid, A.; Grassian, V. H. *The Analyst* **2014**, *139*, 870.

(19) Shang, L.; Yang, L. X.; Seiter, J.; Heinle, M.; Brenner-Weiss, G.; Gerthsen, D.; Nienhaus, G. U. *Advanced Materials Interfaces* **2014**, *1*, n/a.

(20) Hellstrand, E.; Lynch, I.; Andersson, A.; Drakenberg, T.; Dahlback, B.; Dawson, K. A.; Linse, S.; Cedervall, T. *FEBS Journal* **2009**, *276*, 3372.

(21) Podila, R.; Brown, J. M.; Kahru, A.; Rao, A. M. *Mrs Bulletin* **2014**, *39*, 990.

(22) Saptarshi, S. R.; Duschl, A.; Lopata, A. L. *Journal of Nanobiotechnology* **2013**, *11*, 26.

(23) Xu, M.; Li, J.; Iwai, H.; Mei, Q.; Fujita, D.; Su, H.; Chen, H.; Hanagata, N. *Scientific Reports* **2012**, *2*, 406.

(24) El Kadi, N.; Taulier, N.; Le Huerou, J. Y.; Gindre, M.; Urbach, W.; Nwigwe, I.; Kahn, P. C.; Waks, M. *Biophysical Journal* **2006**, *91*, 3397.

(25) Fukuzaki, S.; Urano, H.; Nagata, K. *Journal of Fermentation and Bioengineering* **1996**, *81*, 163.

(26) Larsericsdotter, H.; Oscarsson, S.; Buijs, J. *Journal of Colloid and Interface Science* **2005**, *289*, 26.

(27) Wassell, D. T.; Embery, G. *Biomaterials* **1996**, *17*, 859.

(28) Wiśniewska, M.; Szewczuk-Karpisz, K.; Sternik, D. *Journal of Thermal Analysis and Calorimetry* **2014**, *120*, 1355.

(29) McClellan, S. J.; Franses, E. I. *Colloids and Surfaces, A* **2005**, *260*, 265.
(30) Su, T. J.; Lu, J. R.; Thomas, R. K.; Cui, Z. F.; Penfold, J. *Journal of Physical Chemistry B* **1998**, *102*, 8100.
(31) Schmaljohann, D. *Advanced Drug Delivery Reviews* **2006**, *58*, 1655.
(32) Reed, R. G.; Putnam, F. W.; Peters, T. *Biochemical Journal* **1980**, *191*, 867.
(33) Dominguez-Medina, S.; Blankenburg, J.; Olson, J.; Landes, C. F.; Link, S. *ACS Sustainable Chemistry & Engineering* **2013**, *1*, 833.
(34) Jachimska, B.; Pajor, A. *Bioelectrochemistry* **2012**, *87*, 138.
(35) Carter, D. C.; Ho, J. X. *Advanced Protein Chemistry* **1994**, *45*, 153.
(36) Roach, P.; Farrar, D.; Perry, C. C. *Journal of the American Chemical Society* **2006**, *128*, 3939.
(37) Shang, L.; Wang, Y.; Jiang, J.; Dong, S. *Langmuir* **2007**, *23*, 2714.
(38) Ge, S.; Kojio, K.; Takahara, A.; Kajiyama, T. *Journal of Biomaterials Science, Polymer Edition* **1998**, *9*, 131.
(39) Baker, M. J.; Trevisan, J.; Bassan, P.; Bhargava, R.; Butler, H. J.; Dorling, K. M.; Fielden, P. R.; Fogarty, S. W.; Fullwood, N. J.; Heys, K. A.; Hughes, C.; Lasch, P.; Martin-Hirsch, P. L.; Obinaju, B.; Sockalingum, G. D.; Sule-Suso, J.; Strong, R. J.; Walsh, M. J.; Wood, B. R.; Gardner, P.; Martin, F. L. *Nature Protocols* **2014**, *9*, 1771.
(40) Yang, H.; Yang, S.; Kong, J.; Dong, A.; Yu, S. *Nature Protocols* **2015**, *10*, 382.
(41) Chittur, K. K. *Biomaterials* **1998**, *19*, 357.
(42) Steiner, G.; Tunc, S.; Maitz, M.; Salzer, R. *Analytical Chemistry* **2007**, *79*, 1311.
(43) Lehman, S. E.; Mudunkotuwa, I. A.; Grassian, V. H.; Larsen, S. C. *Langmuir* **2016**, *32*, 731.
(44) Saha, B.; Das, G. *Journal of Physical Chemistry C* **2009**, *113*, 15667.
(45) Demanèche, S.; Chapel, J.-P.; Monrozier, L. J.; Quiquampoix, H. *Colloids and Suraces., B* **2009**, *70*, 226.
(46) Kosmulski, M. *Journal of Colloid and Interface Science* **2002**, *253*, 77.
(47) Fu, F.-N.; DeOliveira, D. B.; Trumble, W. R.; Sarkar, H. K.; Singh, B. R. *Applied Spectroscopy* **1994**, *48*, 1432.
(48) Kong, J.; Yu, S. *Acta Biochimica et Biophysica Sinica* **2007**, *39*, 549.
(49) Moulton, S. E.; Barisci, J. N.; McQuillan, A. J.; Wallace, G. G. *Colloids and Surfaces, A* **2003**, *220*, 159.
(50) Schwinte, P.; Voegel, J.-C.; Picart, C.; Haikel, Y.; Schaaf, P.; Szalontai, B. *Journal Physical Chemistry B* **2001**, *105*, 11906.
(51) Mudunkotuwa, I. A.; Grassian, V. H. *Langmuir* **2014**, *30*, 8751.
(52) Barth, A. *Biochimica et Biophysica Acta* **2007**, *1767*, 1073.
(53) Qing, H.; Yanlin, H.; Fenlin, S.; Zuyi, T. *Spectrochimica Acta Part A: Molecular and Biomolecular Spectroscopy* **1996**, *52*, 1795.
(54) Zeng, H.; Chittur, K. K.; Lacefield, W. R. *Biomaterials* **1999**, *20*, 377.
(55) Kang, Y.; Li, X.; Tu, Y. Q.; Wang, Q.; Agren, H. *Journal of Physical Chemistry C* **2010**, *114*, 14496.
(56) Xu, Y.; Sherwood, J.; Qin, Y.; Crowley, D.; Bonizzoni, M.; Bao, Y. *Nanoscale* **2014**, *6*, 1515.
(57) Bouhekka, A.; Bürgi, T. *Applied Surface Science* **2012**, *261*, 369.
(58) Wright, A. K.; Thompson, M. R. *Biophysical Journal* **1975**, *15*, 137.
(59) Gulseren, I.; Guzey, D.; Bruce, B. D.; Weiss, J. *Ultrasonics Sonochemistry* **2007**, *14*, 173.
(60) Murayama, K.; Wu, Y. Q.; Czarnik-Matusewicz, B.; Ozaki, Y. *Journal of Physical Chemistry B* **2001**, *105*, 4763.

(61) Peters, T., Jr. *All About Albumin: Biochemistry, Genetics, and Medical Applications*; Academic Press, 1995.
(62) Takeda, K.; Wada, A.; Yamamoto, K.; Moriyama, Y.; Aoki, K. *Journal of Protein Chemistry* **1989**, *8*, 653.
(63) Nakamura, K.; Era, S.; Ozaki, Y.; Sogami, M.; Hayashi, T.; Murakami, M. *FEBS Letters* **1997**, *417*, 375.
(64) Sogami, M.; Foster, J. R. *Biochemistry* **1968**, *7,* 2172.
(65) Giacomelli, C. E.; Norde, W. *Journal of Colloid and Interface Science* **2001**, *233*, 234.
(66) Norde, W.; Favier, J. P. *Colloids and Surfaces* **1992**, *1,* 87.
(67) Rimola, A.; Costa, D.; Sodupe, M.; Lambert, J. F.; Ugliengo, P. *Chemical Reviews* **2013**, *113*, 4216.
(68) Mueller, R.; Kammler, H. K.; Wegner, K.; Pratsinis, S. E. *Langmuir* **2003**, *19*, 160.
(69) Hong, Y.; Yu, M.; Lin, J.; Cheng, K.; Weng, W.; Wang, H. *Colloids and Surfaces B, Biointerfaces* **2014**, *123*, 68.
(70) Kubiak-Ossowska, K.; Mulheran, P. A. *Langmuir* **2010**, *26*, 7690.
(71) Fleischer, C. C.; Payne, C. K. *Accounts of Chemical Research* **2014**, *47*, 2651.
(72) Norde, W. *Colloids and Surfaces B, Biointerfaces* **2008**, *61*, 1.
(73) Lee, Y. K.; Choi, E. J.; Webster, T. J.; Kim, S. H.; Khang, D. *International Journal of Nanomedicine* **2015**, *10*, 97.
(74) Kurrat, R.; Prenosil, J. E.; Ramsden, J. J. *Journal of Colloid and Interface Science* **1997**, *185*, 1.
(75) Feng, B.; Weng, J.; Yang, B. C.; Chen, J. Y.; Zhao, J. Z.; He, L.; Qi, S. K.; Zhang, X. D. *Materials Characterization* **2002**, *49*, 129.
(76) Castillo, R.; Koch, B.; Ruiz, P.; Delmon, B. *Journal of Materials Chemistry* **1994**, *4*, 903.
(77) Wälivaara, B.; Aronsson, B.-O.; Rodahl, M.; Lausmaa, J.; Tengvall, P. *Biomaterials* **1994**, *15*, 827.
(78) Ohno, T.; Sarukawa, K.; Tokieda, K.; Matsumura, M. *Journal of Catalysis* **2001**, *203*, 82.
(79) Hurum, D. C.; Agrios, A. G.; Gray, K. A.; Rajh, T.; Thurnauer, M. C. *The Journal of Physical Chemistry B* **2003**, *107*, 4545.

Graphical Abstract